Applied Physics Letters

RESEARCH ARTICLE | SEPTEMBER 09 2025

Evaluation of exchange stiffness constant in iron garnet film using micromagnetic simulation

Takumi Koguchi ; Toshiaki Watanabe ; Hibiki Miyashita ; Kazushi Ishiyama ; Yuichi Nakamura ; Mitsuteru Inoue ; Mehmet C. Onbasli ; Taichi Goto

Check for updates

Appl. Phys. Lett. 127, 102407 (2025)
https://doi.org/10.1063/5.0283742

View Online
Export Citation

Articles You May Be Interested In

Photoluminescence study of magnetic spin clusters and their temperature evolution in $Cd_{0.70}Mn_{0.30}Te$ spin-glass compound

J. Appl. Phys. (November 2012)

Growth of magnetooptical cerium-substituted yttrium iron garnet on yttrium aluminum garnet using ion beam sputtering

Appl. Phys. Lett. (September 2023)

Thermal observables in coupled Cr_7Ni molecular rings: Role and quantification of spin-entanglement

J. Appl. Phys. (March 2011)

10 March 2026 10:38:58

AIP Advances
Why Publish With Us?
21DAYS average time to 1st decision
OVER 4 MILLION views in the last year
INCLUSIVE scope
Learn More
AIP Publishing

AIP Publishing

Applied Physics Letters ARTICLE pubs.aip.org/aip/apl

Evaluation of exchange stiffness constant in iron garnet film using micromagnetic simulation

Cite as: Appl. Phys. Lett. **127**, 102407 (2025); doi: 10.1063/5.0283742
Submitted: 3 June 2025 · Accepted: 29 July 2025 ·
Published Online: 9 September 2025

View Online Export Citation CrossMark

Takumi Koguchi,[1,2,3] Toshiaki Watanabe,[4] Hibiki Miyashita,[1,2] Kazushi Ishiyama,[1] Yuichi Nakamura,[3] Mitsuteru Inoue,[1] Mehmet C. Onbasli,[5] and Taichi Goto[1,a)]

AFFILIATIONS

[1]Research Institute of Electrical Communication, Tohoku University, 2-1-1 Katahira, Aoba, Sendai, Miyagi 980-8577, Japan
[2]Graduate School of Engineering, Tohoku University, 6-6 Aramaki, Aoba, Sendai, Miyagi 980-8579, Japan
[3]Toyohashi University of Technology, 1-1 Hibarigaoka, Tempaku, Toyohashi, Aichi 441-8580, Japan
[4]Shin-Etsu Chemical Co., Ltd., 2-13-1 Isobe, Annaka, Gunma 379-0195, Japan
[5]Electrical and Electronics Engineering and Physics, Koç University, Rumelifeneri Yolu 34450, Sariyer, Istanbul, Turkey

[a)]**Author to whom correspondence should be addressed:** taichi.goto.a6@tohoku.ac.jp. **Tel.:** +81-22-217-5489

ABSTRACT

Measurement of exchange stiffness constants (ESCs) is crucial for describing magnetization phenomena. Large-scale micromagnetic simulations (MMSs) are used to determine the ESC of iron garnet thin films exhibiting perpendicular magnetic anisotropy. The ESC determined by fitting the calculated domain periodicity with experimental data acquired through a polarized microscope is comparable to previously reported values. In addition, the simulations showed mixed-configuration domain wall (DW) structure with a large Néel–Bloch DW ratio. This study demonstrates the capability of MMS for evaluating ESCs while providing additional insights into DW physics, offering a facile approach for describing spin dynamics in magnetic garnets.

© 2025 Author(s). All article content, except where otherwise noted, is licensed under a Creative Commons Attribution (CC BY) license (https://creativecommons.org/licenses/by/4.0/). https://doi.org/10.1063/5.0283742

10 March 2026 10:38:58

Magnetic garnets are key materials in a wide range of fields because of their unique magnetic and magnetooptical (MO) properties.[1–7] They are widely used in MO devices such as optical isolators,[8–12] modulators,[13,14] memories,[15,16] and field indicators[17–19] as well as in spintronic[20–23] and magnonic devices.[3,24–28] In these magnetic garnet films, the exchange stiffness constant (ESC), A_{ex}, which quantifies the coupling strength between magnetic moments in magnetic materials, plays a crucial role in determining the magnetic domain structures and magnetic dynamic responses in magnetic garnet films. Several methods have been proposed for determining the ESC, including observing domain wall (DW) widths (w_{DW}) using an MO microscope and deriving the ESC based on the equation $A_{ex} = K_U(w_{DW}/\pi)^2$, where K_U is the magnetic anisotropy energy (MAE).[29] However, precise observation of ten-nanometer-order DW width of iron garnet using a microscope is challenging because of camera resolution and diffraction limit. Nam *et al.* demonstrated an ESC measurement method based on DW chirality transitions.[29] On injecting a spin-transfer torque into a Co wire with a thickness of 0.5–0.8 nm and width of 20 μm fabricated by photolithography, the system shows good spin–orbital torque efficiency and DW widths while yielding ESCs within 2.9–10 pJ/m. However, this method requires a lithography process that damages the sample. Klingler *et al.* report the ESC measurement of 0.8–2.6 μm-thick non-processed yttrium iron garnet (YIG) films (3.7 pJ/m) using perpendicular standing spin waves (PSSWs) under a magnetic field of $<$880 mT.[30] However, this method cannot be used for $\sim$100 nm thick films as it requires a magnetic field $>$10 T to excite sufficient number of PSSW peaks. Matsumoto *et al.* used Brillouin light scattering (BLS) to determine the ESC of a 140-μm-thick bismuth-substituted YIG (Bi:YIG) film (3.87 pJ/m).[31] This method required a large-scale resonant optical setup to observe BLS peaks. Hence, we propose a simple method for determining A_{ex} using micromagnetic simulations (MMSs)[32–35] fitted to experimentally observed domain features, overcoming the limitations of current ESC determination methods. Unlike conventional approaches that require sophisticated instrumentation, our method achieves accurate ESC determination using only a microscope and computational analysis.

A 129 nm-thick single-crystalline cerium-substituted YIG (Ce:YIG, $Ce_{0.9}Y_{2.1}Fe_5O_{12-\delta}$) film grown on a garnet substrate exhibiting perpendicular magnetic anisotropy (PMA) and out-of-plane (OP) magnetic domains was used for analysis. The film was deposited using radio frequency ion beam sputtering (RF-IBS) on (111)-oriented

© Author(s) 2025

gadolinium gallium garnet (GGG). The film thickness t was 129 ± 4.5 nm, measured by stylus profilometer (KLA Alpha-Step IQ). The error represents the standard deviation of nine repeated measurements. The saturation magnetization of 135 ± 5 kA/m was measured at room temperature (~27 °C) using a vibrating-sample magnetometer (VSM, Tamakawa TM-VSM2050-HGC-TOH), showing MAE K_U of $1.49 \pm 0.05 \times 10^4$ J/m^3, magnetostatic (MS) anisotropy K_{MS} of $-2\pi M_s^2 = -1.15 \pm 0.08 \times 10^4$ J/m^3, and MAE excluding K_{MS} of $2.64 \pm 0.13 \times 10^4$ J/m^3. A magnetic domain image was obtained at room temperature using MO Faraday effect (MOFE, Neoark MD-800TG) microscope (Fig. 1) after AC demagnetization, showing a domain half-period (w_{D+DW}; i.e., the sum of w_D and w_{DW}) of 352 ± 18 nm. The values of w_D and w_{DW} remain unseparated because of the spatial resolution of the microscope. The error represents the standard deviation obtained from measurements at ten different points in the acquired image.

This magnetic domain image, represented by the domain half-period, was replicated by three-dimensional (3D) MMS with the EXAMAG simulation software (Fujitsu, Solver version 2.3.d58, GUI version 2.3.d58). The model size of the magnetic material, assuming Ce:YIG, was set to $5 \times 5\ \mu m^2$ to ensure at least 10 domain half-periods. The thickness was varied from 110 to 150 nm. The cell size was set to 10 nm^3, and an air region of $40 \times 40 \times 40\ \mu m^3$ was added for stray field calculations with gradually increasing cell sizes in air. As a result, the number of cells was between 2.75×10^6 and 3.75×10^6 for the magnetic material and between 2.42×10^7 and 2.52×10^7 in total. Large parallel computing on two cluster systems, namely, AOBA-B (Tohoku University) using 128 CPU cores and 256 GB of memory and Fugaku (RIKEN) using 144 CPU cores and 96 GB of memory, was used to simulate the large model in this study. An energy-minimization method was used to calculate the magnetic domain structure, corresponding to the steady-state solution of the Landau–Lifshitz–Gilbert equation. This method calculates the directions of the magnetization vectors of all cells to minimize the total energy of the entire model, including the magnetocrystalline (MC) anisotropy, MS anisotropy, exchange, and Zeeman energies. The temperature effect was not taken into account due to its negligible influence on the DW state as shown in Fig. S1 in the supplementary material. The Dzyaloshinskii–Moriya interaction (DMI) was not considered in this simulation because of its negligible contribution at the relatively large thickness of 130 nm, since DMI scales inversely with thickness.[36] Energy minimization was conducted using the nonlinear conjugate gradient method with a convergence threshold of 1.0×10^{-6}, and static magnetic field calculations were conducted using the conjugate gradient method with a threshold of 1.0×10^{-7}. The initial magnetization directions were randomized to represent the magnetic state after the AC magnetization cycle in the experiment, and the material parameters measured experimentally (summarized in Table I) were used in the simulation. The ESC of the magnetic material layer was varied from 2 to 8 pJ/m, thereby modifying the magnetic domain state (Fig. 2).

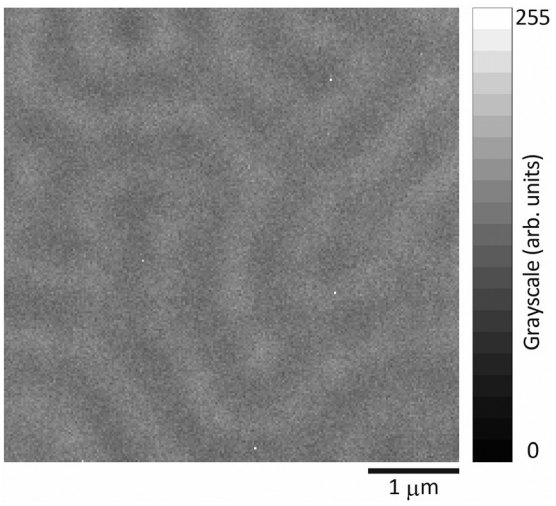


FIG. 1. MOFE image of a central area ($5 \times 5\ \mu m^2$) on the Ce:YIG film observed without magnetic field at a wavelength of 470 nm.

The domain half-periods w_{D+DW} (black dots) of Ce:YIG films with various ESCs obtained from simulated domain patterns are shown in Fig. 2(a). The error bars show the deviation of w_{D+DW} from ten domains; Figs. 2(b)–2(h) show the magnetization distribution along the z direction at the model surface. Maze-type magnetic domain structures with PMA were obtained for all cases. The w_{D+DW} of 344 ± 55 nm [Fig. 2(d)] calculated with A_{ex} of 4 pJ/m is the closest to the experimental value (352 ± 18 nm). Considering the experimental variation in the w_{D+DW} values, A_{ex} of the fabricated Ce:YIG film lies in the range 3.8–4.4 pJ/m. The calculation error arises from simulation–experiment discrepancies in partial bubble domain structure and MS anisotropy, reducible with larger simulation models.

The theoretical value of w_{D+DW} (red line in Fig. 2) can be calculated using Eq. (1) showing domain energy ε proposed by Kooy and Enz[37] assuming a pure Néel DW, where the auxiliary variable g is $t\sqrt{\mu^*}/2w_D\mu^*$, μ^* is $1 + M_S^2/2\mu_0 K_U$, and μ_0 is the vacuum permeability. The w_D value is obtained by minimizing ε,

$$\varepsilon = \frac{8M_S^2 w_D}{\pi^3 \mu_0} \sum_{n=\text{odd}}^{\infty} \frac{1}{n^3} \frac{\sinh(n\pi g)}{\sinh(n\pi g) + \sqrt{\mu^*}\cos(n\pi g)} + 4\sqrt{A_{ex}K_U}\frac{t}{w_D}. \quad (1)$$

The first and second terms denote the magnetic domain and DW energies, respectively. These values are in good agreement with those obtained by 3D MMS and best reproduce the experimental ESC value of 3.8 pJ/m. The ESC values estimated from 3D MMS (3.8–4.4 pJ/m) and calculated using Eq. (1) (3.8 pJ/m) are consistent with the former reported values of ESC for 0.9–2.6 μm-thick YIG (3.7 ± 0.4 pJ/m)[30]

TABLE I. Measured physical constants of the deposited Ce:YIG film used in the determination of ESC.

Physical constant	Value
Thickness, t	129 ± 4.5 nm
Saturation magnetization, M_s	135 ± 5 kA/m
MAE, K_U	$1.49 \pm 0.05 \times 10^4$ J/m^3
MS anisotropy, K_{MS}	$-1.15 \pm 0.08 \times 10^4$ J/m^3
MAE excluding K_{MS}, K_U^{MM}	$2.64 \pm 0.13 \times 10^4$ J/m^3
Domain half-period, w_{D+DW}	352 ± 18 nm

10 March 2026 10:38:58

© Author(s) 2025

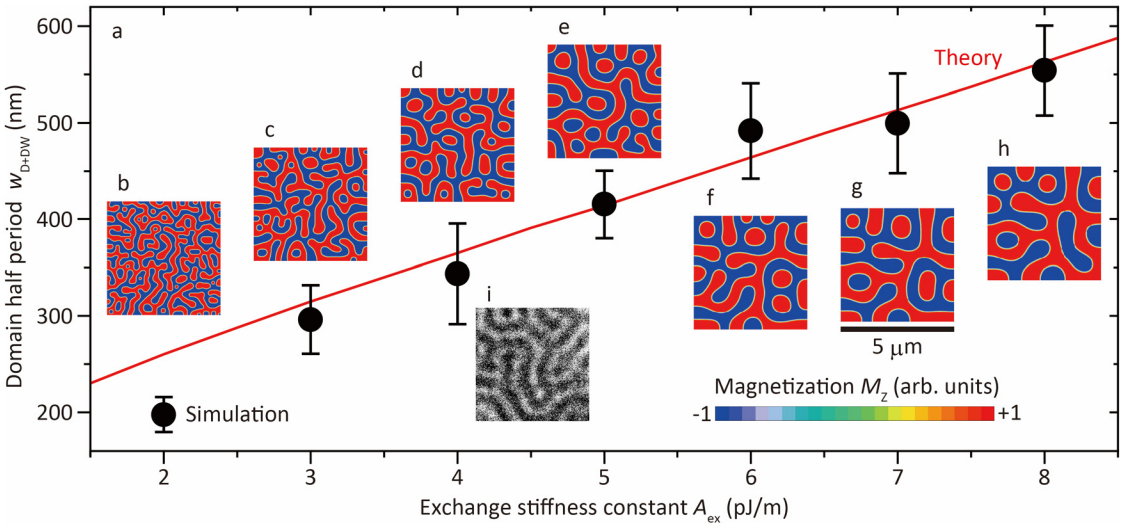


FIG. 2. (a) Domain half-period w_{D+DW} vs the ESC A_{ex}. The black dots and error bars represent the average and standard deviation of w_{D+DW}, respectively. The red line shows the results of calculation using Kooy's equation[37] assuming a pure Néel DW. The square contour maps show the OP magnetization distribution at the magnetic layer surface for the following ESC, A_{ex}, values: (b) 2 pJ/m, (c) 3 pJ/m, (d) 4 pJ/m, (e) 5 pJ/m, (f) 6 pJ/m, (g) 7 pJ/m, and (h) 8 pJ/m. (i) To facilitate comparison, we reprint the experimental data from Fig. 1 with adjusted contrast.

and 1 μm-thick $Y_{2.0}Ca_{1.0}Ge_{0.9}Fe_{4.1}O_{12}$ (3.5 pJ/m).[38] The largest discrepancy obtained at $A_{ex} = 2$ pJ/m was due to the insufficient separation between the calculation mesh size (10 nm) and the characteristic length $\sqrt{A_{ex}/K_U}$ of ~12 nm. A smaller mesh size and larger computational resources would solve this issue.

Figure 3 shows vector maps of the magnetization near DWs in cross-sectional views for different values of ESCs: (a) 2 pJ/m, (b) 4 pJ/m, (c) 6 pJ/m, and (d) 8 pJ/m. The value of M_x varies at the thickness center, and the M_y lies near the surface, indicating that the DWs are neither simple Néel nor Bloch walls. Such DWs, known as mixed-configuration

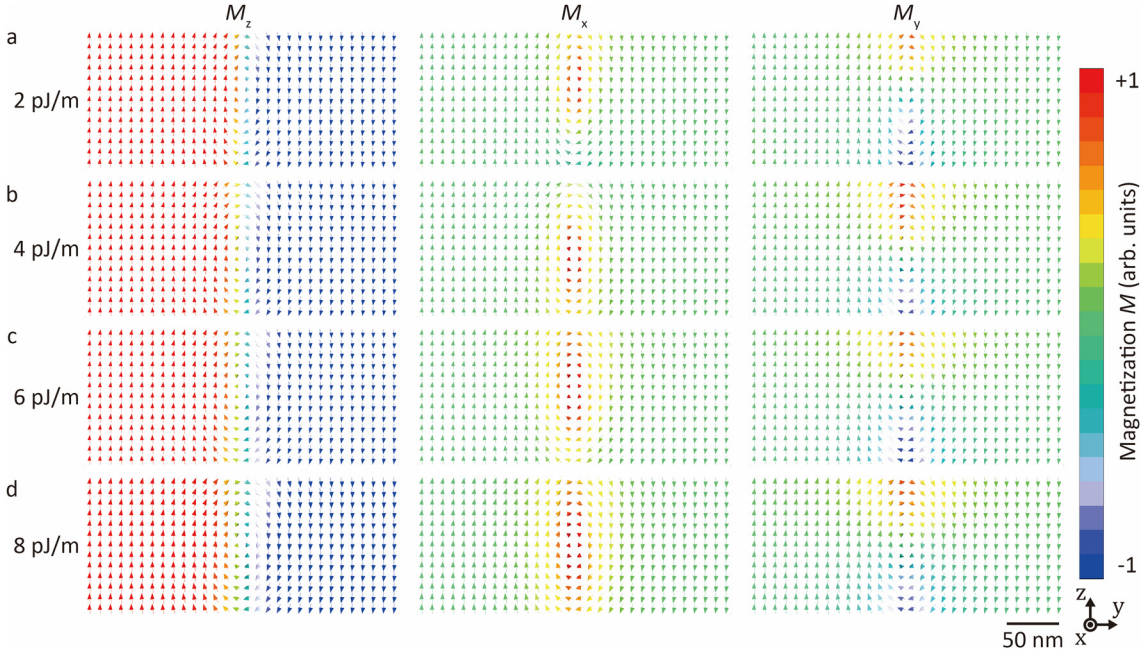


FIG. 3. Cross-sectional views of simulated DWs for the following ESCs: (a) 2 pJ/m, (b) 4 pJ/m, (c) 6 pJ/m, and (d) 8 pJ/m. The center of each image corresponds to a DW. The arrows indicate the direction of magnetization vectors comprising M_x, M_y, and M_z. The color of each arrow represents the magnitude of the respective magnetization component; the directions and lengths of all arrows are the same.

10 March 2026 10:38:58

© Author(s) 2025

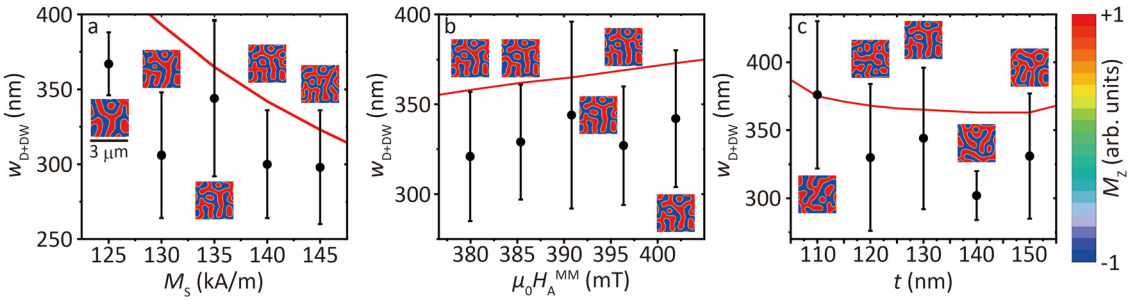


FIG. 4. Plots of w_{D+DW} vs the (a) saturation magnetization M_S, (b) magnetic anisotropy field $\mu_0 H_A^{MM}$, and (c) film thickness t. Black dots represent the average values, and error bars indicate the standard deviations. Red lines represent theoretical values calculated using Eq. (1). Square contour maps show the magnetic domain structures at the sample surface; the color scale corresponds to the magnetization component along the OP direction M_z.

walls or cross-tie walls,[39] are observed in thin films.[6,40] Notably, the w_{DW} does not change significantly with increasing ESC. Moreover, the w_{DW} at $A_{ex} = 4$ pJ/m at the surface (approximately 50 ± 20 nm) obtained using a Boltzmann-sigmoid function fitting[41] is consistent with the theoretical value of 51 nm derived from $w_{DW} = \pi\sqrt{A_{ex}/K_U}$ assuming pure Néel DWs.[39] MMSs show details of the structure and DW width that cannot be clearly identified through experimental observations. The DW structures simulated using the other ESCs are shown in Fig. S2.

To confirm the validity of the ESC determination strategy reported here, the influence of the deviation of other material parameters on the domain structure was investigated. The variation in w_{D+DW} on varying the saturation magnetization M_S, magnetic anisotropy field H_A^{MM}, and sample thickness t is shown in Fig. 4. The following were used as fixed values: $M_S = 135$ kA/m, $H_A^{MM} = 391$ mT, $t = 130$ nm, and ESC $A_{ex} = 4$ pJ/m. The red line in the figure represents the theoretical values calculated using Eq. (1). A smaller M_S leads to a larger w_{D+DW}, likely owing to an increase in K_U favoring the OP easy axis [Fig. 4(a)]. The influence of the magnetic anisotropy field H_A^{MM} on experimental fluctuations is presented in Fig. 4(b), which shows a slight increase in the domain half-period. The minor influence of film thickness is shown in Fig. 4(c). These results indicate a weaker dependence of fluctuations in M_S, H_A^{MM}, and t on w_{D+DW} compared with A_{ex}.

The MAE derived from the magnetic hysteresis loops at $A_{ex} = 4$ pJ/m (1.52×10^4 J/m^3) is similar to the experimental value of MAE listed in Table I (1.49×10^4 J/m^3) [Fig. 5(a)], although the calculated loop looks different from the measured hysteresis as shown in Fig. S3. The maze magnetic domains of M_z under OP and IP fields are shown in Figs. 5(b)–5(f) and 5(g)–5(l), respectively. During the initial OP and IP magnetization processes, the maze and stripe magnetic domains gradually disappear. Coercivities of 33 and 14 mT are experimentally measured for the Ce:YIG films in the IP and OP directions, respectively, using a VSM. The experimentally measured and calculated values in the IP direction are consistent, but those in the OP direction differ as shown in Fig. S3. This discrepancy is attributed to idealized material structures in simulations, which differ from the real

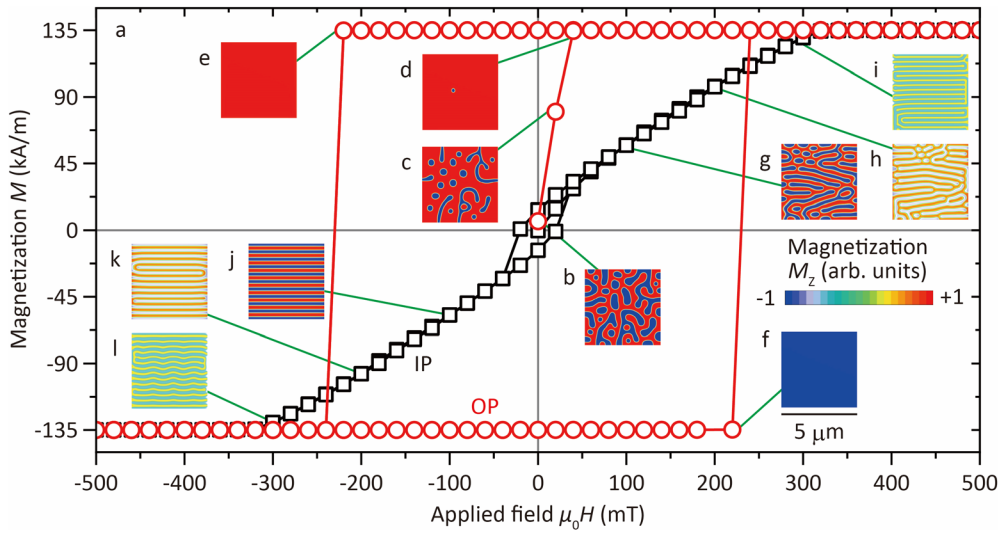


FIG. 5. (a) OP and IP magnetic hysteresis loops at $A_{ex} = 4$ pJ/m. Red and black circles represent the OP and IP loops. (b)–(f) Magnetic domain images showing OP magnetization under an OP field at (b) 0 mT, (c) +20 mT, (d) +40 mT, (e) –220 mT, and (f) +220 mT. (g)–(l) Magnetic domain images showing OP magnetization under an IP field: at (g) +100 mT, (h) +200 mT, (i) +300 mT, (j) –100 mT, (k) –200 mT, and (l) –300 mT.

10 March 2026 10:38:58

© Author(s) 2025

structures of experimental materials. Therefore, these results suggest that structural improvements in the experimental sample to make it more similar to the simulated system would increase its OP coercivity. Other hysteresis loops simulated using different ESCs are shown in Fig. S4.

In conclusion, 3D MMS enabled the evaluation of the ESC, A_{ex}, in an epitaxially grown single-crystalline Ce:YIG film using polarized microscope images. Through these simulations, the ESC was determined to be between 3.8 and 4.4 pJ/m, consistent with previously reported experimental values for magnetic garnet materials. The accuracy of this ESC determination would be improved by larger-scale simulations, clearer magnetic domain observations using shorter-wavelength light sources (e.g., radiation facilities), and advanced image similarity evaluation not limited to the domain half periodicity. The demonstrated method can be generalized to other domain-observable magnetic materials, including metals and multilayer structures. The calculated magnetic hysteresis loops indicated discrepancies between experiment and calculation, particularly related to OP coercivity factors such as structural uniformity and/or anisotropy energy distributions. Simultaneously, the usability of the 2D theoretical model assuming Néel DW was demonstrated. In contrast, 3D simulation results showed mixed-configuration domain structure, difficult to access through experiments or conventional 2D theoretical models alone. Thus, the simple MMS-based ESC determination method established in this study complements classical theoretical ESC estimation strategies without requiring sophisticated instrumentation or complicated processes, making it useful for obtaining ESC and designing DW-based devices[42] and magnonic devices.[23] This study provides deeper insights into the magnetic properties of garnet films and paves the way for developing functional magnetooptical and spintronic applications.

See the supplementary material for the following details: comparison of calculation methods with and without thermal effects (Fig. S1); cross-sectional views of domain walls for different ESCs (Fig. S2); measured magnetic hysteresis loops of Ce:YIG film (Fig. S3); calculated OP magnetic hysteresis loops for various ESCs (Fig. S4).

This work was partly supported by JSPS KAKENHI (Nos. 23H01439, and 23K17758), JSPS Bilateral Joint Research (No. JPJSBP120249401), NEDO (No. 23200047), the Amada Foundation. T.G., T.K., and H.M. acknowledge receiving support through fellowships provided by TI-FRIS and JST SPRING (No. JPMJSP2114), respectively. M.C.O. acknowledges ERC (No. 948063) and TUBITAK Bilateral Collaboration Grant (No. 223N037). We also acknowledge receiving support from TU-FTC, TU-LNS, TU-CINTS, TU-GIMRT, TU-CC, and HPCI (No. hp240340).

AUTHOR DECLARATIONS

Conflict of Interest

The authors have no conflicts to disclose.

Author Contributions

Takumi Koguchi: Data curation (lead); Formal analysis (equal); Software (lead); Writing – original draft (supporting). **Toshiaki Watanabe:** Data curation (supporting); Investigation (supporting). **Hibiki Miyashita:** Data curation (supporting); Validation (supporting). **Kazushi Ishiyama:** Supervision (supporting); Validation (supporting). **Yuichi Nakamura:** Data curation (supporting); Supervision (supporting). **Mitsuteru Inoue:** Funding acquisition (equal); Validation (supporting). **Mehmet Cengiz Onbasli:** Data curation (supporting); Validation (lead). **Taichi Goto:** Conceptualization (lead); Formal analysis (equal); Funding acquisition (equal); Project administration (equal); Software (equal); Supervision (lead); Writing – original draft (lead); Writing – review & editing (lead).

DATA AVAILABILITY

The data that support the findings of this study are available within the article and its supplementary material.

REFERENCES

[1]P. Hansen and J. P. Krumme, "Magnetic and magneto-optical properties of garnet films," Thin Solid Films **114**(1–2), 69 (1984).
[2]Y. Yang, T. Liu, L. Bi *et al.*, "Recent advances in development of magnetic garnet thin films for applications in spintronics and photonics," J. Alloys Compd. **860**, 158235 (2021).
[3]B. Flebus, D. Grundler, B. Rana *et al.*, "The 2024 magnonics roadmap," J. Phys.: Condens. Matter **36**(36), 363501 (2024).
[4]J. Smit and H. P. J. Wijn, *Ferrites* (Cleaver-Hume Press, London, 1959).
[5]A. H. Eschenfelder, *Magnetic Bubble Technology* (Springer-Verlag, Berlin, 1981).
[6]A. Hubert and R. Schafer, *Magnetic Domains: The Analysis of Magnetic Microstructures* (Springer, Berlin, 1998).
[7]Y. Yoshihara, K. Ishiyama, T. Watanabe *et al.*, "Growth of magnetooptical cerium-substituted yttrium iron garnet on yttrium aluminum garnet using ion beam sputtering," Appl. Phys. Lett. **123**(11), 112404 (2023).
[8]L. Bi, J. Hu, P. Jiang *et al.*, "On-chip optical isolation in monolithically integrated non-reciprocal optical resonators," Nat. Photonics **5**, 758 (2011).
[9]B. J. H. Stadler and T. Mizumoto, "Integrated magneto-optical materials and isolators: A review," IEEE Photonics J. **6**(1), 1–15 (2014).
[10]J. Lapointe, C. Coia, A. Dupont *et al.*, "Passive broadband Faraday isolator for hybrid integration to photonic circuits without lens and external magnet," Nat. Photonics **19**, 248 (2025).
[11]Y. Yang, T. Zhang, D. Wu *et al.*, "Europium-substituted cerium iron garnet thin films for silicon-integrated nonreciprocal photonic device applications," APL Mater. **13**(5), 051109 (2025).
[12]M. Levy, R. M. Osgood, Jr., H. Hegde *et al.*, "Integrated optical isolators with sputter-deposited thin-film magnets," IEEE Photonics Technol. Lett. **8**(7), 903 (1996).
[13]S. Kharratian, H. Urey, and M. C. Onbaşlı, "Advanced materials and device architectures for magnetooptical spatial light modulators," Adv. Opt. Mater. **8**(1), 1901381 (2020).
[14]T. Goto, R. Morimoto, J. W. Pritchard *et al.*, "Magneto-optical Q-switching using magnetic garnet film with micromagnetic domains," Opt. Express **24**(16), 17635 (2016).
[15]R. S. Mezrich, "Magnetic holography," Appl. Opt. **9**(10), 2275 (1970).
[16]R. Isogai, S. Suzuki, K. Nakamura *et al.*, "Collinear volumetric magnetic holography with magnetophotonic microcavities," Opt. Express **23**(10), 13153 (2015).
[17]M. Takahashi, K. Kawasaki, H. Ohba *et al.*, "Electromagnetic near field measurements by using magnet garnet crystal," J. Appl. Phys. **107**(9), 09E711 (2010).
[18]T. Ishibashi, T. Kawata, T. H. Johansen *et al.*, "Magneto-optical indicator garnet films grown by metal-organic decomposition method," J. Magn. Soc. Jpn. **32**(2), 150 (2008).
[19]M. Takezawa and J. Yamasaki, "Dynamic domain observation in narrow thin films," IEEE Trans. Magn. **37**(4), 2034 (2001).
[20]E. Y. Vedmedenko, R. K. Kawakami, D. D. Sheka *et al.*, "The 2020 magnetism roadmap," J. Phys. D **53**(45), 453001 (2020).
[21]T. Fakhrul, S. Huang, Y. Song *et al.*, "Influence of substrate on interfacial Dzyaloshinskii-Moriya interaction in epitaxial $Tm_3Fe_5O_{12}$ films," Phys. Rev. B **107**(5), 054421 (2023).

10 March 2026 10:38:58

© Author(s) 2025

[22]C. O. Avci, E. Rosenberg, L. Caretta *et al.*, "Interface-driven chiral magnetism and current-driven domain walls in insulating magnetic garnets," Nat. Nanotechnol. **14**(6), 561 (2019).
[23]Y. Fan, M. J. Gross, T. Fakhrul *et al.*, "Coherent magnon-induced domain-wall motion in a magnetic insulator channel," Nat. Nanotechnol. **18**(9), 1000 (2023).
[24]D. D. Stancil and A. Prabhakar, *Spin Waves* (Springer, New York, 2009).
[25]T. Fischer, M. Kewenig, D. A. Bozhko *et al.*, "Experimental prototype of a spin-wave majority gate," Appl. Phys. Lett. **110**(15), 152401 (2017).
[26]T. Goto, T. Yoshimoto, B. Iwamoto *et al.*, "Three port logic gate using forward volume spin wave interference in a thin yttrium iron garnet film," Sci. Rep. **9**(1), 16472 (2019).
[27]K. Mori, T. Koguchi, T. Watanabe *et al.*, "Orientation-dependent two-dimensional magnonic crystal modes in an ultralow-damping ferrimagnetic waveguide containing repositioned hexagonal lattices of Cu disks," Phys. Rev. Appl. **21**(1), 014061 (2024).
[28]Q. Wang, A. Hamadeh, R. Verba *et al.*, "A nonlinear magnonic nano-ring resonator," npj Comput. Mater. **6**(1), 192 (2020).
[29]Y.-S. Nam, D.-Y. Kim, Y.-K. Park *et al.*, "Exchange-stiffness measurement scheme based on domain-wall chirality transition," Appl. Phys. Lett. **121**(7), 072403 (2022).
[30]S. Klingler, A. V. Chumak, T. Mewes *et al.*, "Measurements of the exchange stiffness of YIG films using broadband ferromagnetic resonance techniques," J. Phys. D **48**(1), 015001 (2015).
[31]K. Matsumoto, T. Brächer, P. Pirro *et al.*, "Optical determination of the exchange stiffness constant in an iron garnet," Jpn. J. Appl. Phys. **57**(7), 070308 (2018).
[32]H. Kronmuller and F. Manfred, *Micromagnetism and the Microstructure of Ferromagnetic Solids* (Cambridge University Press, Cambridge, UK, 2003).
[33]R. Chang, S. Li, M. V. Lubarda *et al.*, "FastMag: Fast micromagnetic simulator for complex magnetic structures (invited)," J. Appl. Phys. **109**(7), 07D358 (2011).
[34]S. Fu, R. Chang, S. Couture *et al.*, "Micromagnetics on high-performance workstation and mobile computational platforms," J. Appl. Phys. **117**(17), 17E517 (2015).
[35]A. Ooba, T. Komine, and R. Sugita, "Micromagnetic study of novel domain wall motion modes in bilayer nanowire with low saturation magnetization," J. Appl. Phys. **113**(20), 203915 (2013).
[36]H. Wang, J. Chen, T. Liu *et al.*, "Chiral spin-wave velocities induced by all-garnet interfacial Dzyaloshinskii-Moriya interaction in ultrathin yttrium iron garnet films," Phys. Rev. Lett. **124**(2), 027203 (2020).
[37]C. Kooy and U. Enz, "Experimental and theoretical study of the domain configuration in thin layers of $BaFe_{12}O_{19}$," Philips Res. Rep. **15**, 7 (1960).
[38]Z.-Q. Han, L. Pust, P. E. Wigen *et al.*, "Critical angle of linear spin wave spectrum of CaGe:YIG film," J. Magn. Magn. Mater. **140-144**, 733 (1995).
[39]S. Chikazumi, *Physics of Ferromagnetism* (Oxford University Press, Oxford, 2009).
[40]J. C. Slonczewski, "Theory of domain-wall motion in magnetic films and platelets," J. Appl. Phys. **44**(4), 1759 (1973).
[41]B. A. Lilley, "LXXI. Energies and widths of domain boundaries in ferromagnetics," London, Edinburgh, Dublin Philos. Mag. J. Sci. **41**(319), 792 (1950).
[42]U. Bauer, S. Emori, and G. S. D. Beach, "Voltage-controlled domain wall traps in ferromagnetic nanowires," Nat. Nanotechnol. **8**(6), 411 (2013).

10 March 2026 10:38:58

© Author(s) 2025